Research on friction stir welding of 5754 aluminum alloy with unequal thickness

Han Ronghao[1,2], Ren Daxin[2,3], Song Gang[2,3], Liu Liming[2,3]

韩荣豪, 任大鑫, 宋刚, 刘黎明

1. School of Materials Science and Engineering, Dalian University of Technology, Dalian 116024, China;
2. Key Laboratory of Liaoning Advanced Welding and Joining Technology, Dalian 116024, China;
3. School of Automotive Engineering, Dalian University of Technology, Dalian 116024, China

Received 4 February 2023; accepted 2 May 2023

Abstract A new structure of 1 + 2 was designed in friction stir welding (FSW) of Al alloy sheet with unequal thickness: a specific sheet with similar composition of base metals (BMs) was placed under the thinner sheet as the supporting sheet so that the BM surfaces could be on a plane. The BMs can also be fully penetrated weld with a stirring pin longer than the thickness of the thin sheet. 2 mm and 1.5 mm thick Al alloy sheets were welded by FSW, and parameters were optimized. The highest welding strength reached 96.07% of the thin base metal. Although a slight thinning phenomenon occurred at the edge of the nugget on the retreating side, the specimen still fractured in the heat-affected zone.

Key words friction stir welding, unequal thickness welding, tensile strength, microstructure, supporting sheet

0 Introduction

Aluminum alloy has high specific strength, low density, good corrosion resistance, and good plasticity[1 − 2]. Many structural parts are composed of aluminum alloy tailor-welded blanks of different materials and thicknesses in aerospace, shipbuilding, and automobile manufacturing[3 − 4], which puts forward the demand for welding unequal thickness aluminum alloys. 5754 aluminum alloy is a typical Al-Mg alloy with good corrosion resistance, excellent welding performance, and easy processing and forming. It has been widely used in automobile manufacturing[5].

There are difficulties in welding aluminum alloy tailor-welded blanks with unequal thicknesses. Arc welding and laser welding are mainly used methods[6 − 7]. Nevertheless, shrinkage pores, solidification cracks, and larger heat-affected zone (HAZ) are easy to produce in arc welding due to the significant heat input of arc welding, resulting in the reduction of joint strength[8 − 9]. It is difficult for laser welding to control the accuracy of direct welding of unequal thick sheets due to the small laser spot diameter. The laser beam absorption rate of aluminum alloy is also relatively low[10]. Primary methods such as powder filling and double-sided welding can obtain higher welding joint strength, but the efficiency is low, and the process is complicated[11].

Friction stir welding (FSW) is a solid-phase welding process that can overcome many defects in fusion welding[12 − 13]. Nevertheless, when the thickness difference of Al alloy sheets is slight (such as 1.5 mm A5052 and 1.6 mm A5J32 Al alloy), Nam-Kyu Kim et al.[14] believed that the welding could be directly carried out the similar thickness sheet process. When the sheet thickness difference is significant, it is difficult for the shoulder in the traditional FSW to act on both sheets simultaneously. If plunge depth increases to make the shoulder contact with both base metal

Foundation item: Project was supported by National Key Research and Development Program of China (2022YFB 4600900) the National Natural Science Foundation of China (Grant No. 52275313) and the Fundamental Research Funds for the Central Universities (Grant No. DUT21LAB133).

Corresponding author: Ren Daxin(1982−), Doctor, Associate Professor. Mainly engaged in light weight body development and manufacturing. E-mail: rendx@dlut.edu.cn

doi: 10.12073/j.cw.20230204001

(BM) surfaces, the insufficient plastic material flow will be caused by the different pressures on both sides. At present, some scholars have studied the welding of aluminum alloy plates with different thicknesses. Kim et al.[14] reported that an optimal welding outcome was achieved with a thickness difference of only 0.1 mm by increasing the shoulder plunge depth to ensure effective contact between the tool shoulder and BMs on both sides. Nevertheless, this approach presents a considerable obstacle when welding sheets with a substantial thickness disparity.

Some scholars have made two unequal-thickness sheets flat on the top surface by adding steel pads on the side of the thin sheet. Avinash et al.[15] examined the influence of welding parameters on mechanical properties and microstructure using this method. Buffa et al.[16] investigated material flow and temperature distribution using the method, which revealed the accumulation of excessive heat on the thinner sheet's side and the non-uniform flow of thermoplastic materials. In addition, some scholars have used inclined workbench or welding tools to weld unequal thickness plates. Buffa et al.[17] investigated the possibility of unequal thickness FSW with an inclined weld tool. And the numerical simulation was also used to improve the welding process[18]. S. Shankar[19] conducted FSW of unequal-thickness aluminum-copper and found that high quality welding can be achieved by inclining the workbench and placing a supporting sheet under the thinner copper sheet. This method achieved a good welding effect, but it required higher welding equipment, and it was still difficult for significant thickness differences.

In this study, an improved proposes was carried out to weld unequal thickness sheets. A specific sheet was placed under the thinner sheet as the supporting plate so that the BM surfaces could be on a plane. The supporting sheet's composition was similar to the unequal thickness sheets, and this paper is called supporting base metal (SBM). The material of the three sheets is identical to that of the equal thickness welding, which avoids the problem of uneven temperature field and plastic material flow caused by thickness difference. A stirring pin that exceeded the thickness of the thin upper sheet was used for welding the SBM and unequal BMs together, which means that the original butt structure (1+1) was transformed into a butt-lap structure (1+2). The size of the SBM was as small as possible so that it can be machined or retained after welding.

This new butt structure can bring some advantages. First, BMs' surfaces on a plane made the welding process similar to equal thickness welding, which was convenient. Second, the BMs can be fully penetrated weld. In traditional FSW, the length of the stirring pin is less than the sheet thickness, so there will be potential defects that the bottom of the sheet cannot be completely welded. In this improved process, this possible defect can be avoided because the pin is longer than the thickness of the thinner BM.

In this paper, the feasibility of the improved process was researched. The unequal thickness of 1.5 mm and 2.0 mm 5 754 Al alloy sheets were welded, and 0.5 mm 5 754 Al alloy sheet was selected as the SBM. The effect of parameters on mechanical properties was investigated, and the microstructure of the welded joints was observed.

1 Experiment materials and methods

The dimensions of the three sheets are 80 mm × 60 mm × 2 mm, 80 mm × 60 mm × 1.5 mm, and 80 mm × 25 mm × 0.5 mm, respectively. The chemical composition and mechanical properties of 5 754 aluminum alloy are shown in Table 1. The schematic diagram of the welding structure is shown in Fig.1. The diameter of the stirring tool shoulder was

Table 1 Chemical composition (wt.%) and mechanical properties of 5754 aluminum alloy

Mg	Mn	Si	Fe	Cr	Zn	Al	Yield strength/MPa	Tensile strength/MPa
2.78	0.35	0.17	0.28	0.12	0.09	96.21	116	221

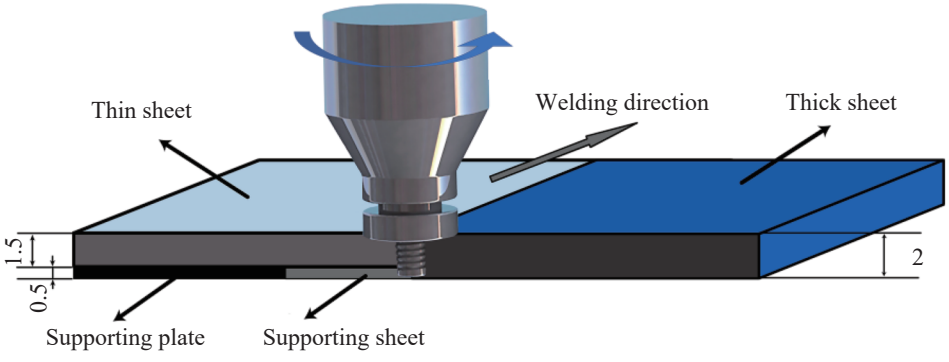

Fig. 1 Schematic diagram of butt-lap joints (mm)

9 mm. The length and diameter of the pin are 1.6 mm and 3 mm, respectively, and the right-handed thread was added.

The orthogonal experiment (OE) was adopted to analyze the effect of welding parameters on mechanical properties. Before the OE, a pre-experiment was carried out to explore the approximate parameters. According to the pre-experimental results, an OE with three factors and five levels was designed, and the details are shown in the following discussion sections.

Tensile strengths of the butt-lap welded joints were tested. A 0.5 mm thick gasket was added when clamping the 1.5 mm thick sheet to avoid the eccentric force caused by the unequal thickness BMs in the tensile experiment. The size and diagram of the tensile specimen are shown in Fig. 2. After the tensile test, a scanning electron microscope (SEM) was used to observe fractures of failure joints.

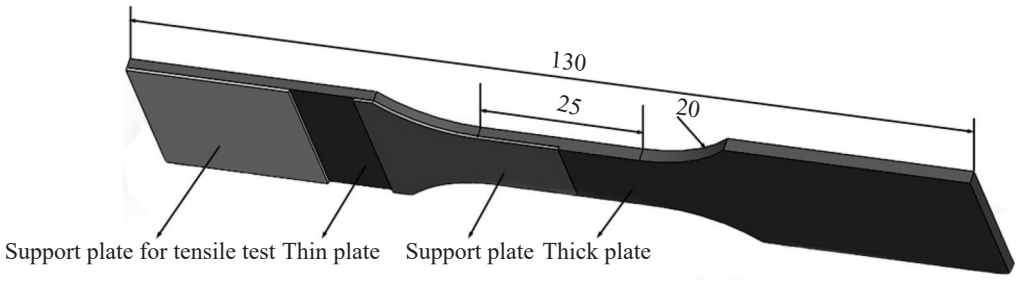

Fig. 2 Schematic diagram of drawing parts size (mm)

After the welding, metallographic specimens of the welded joints were prepared. The cross-section of weld joints was electrolytic polished and anodic coated after ground by sandpaper. The composition of the electrolytic polishing solution and anodic coating solution was $HClO_4$: CH_3CH_2OH at a volume ratio of 1: 9 and HBF_4: H_2O with a volume ratio of 1: 40, respectively. The microstructure was observed by a microscope.

The microhardness test was carried out by a Vickers hardness tester with a load of 500 g and a dwell time of 10 s. The distribution of hardness test points is shown in Fig. 3. The top, middle, and bottom regions were chosen along the transverse direction, 0.25 mm, 1.0 mm, and 1.75 mm from the upper surface of the specimen, respectively. The distance between the test points was 0.5 mm. In the longitudinal direction microhardness tests, the left, middle, and right sides were selected along the longitudinal direction. The distance between the left and right sides from the center of the weld seam was 2.5 mm, and the middle test point was located in the center of the weld seam. And the distance between the test points was 0.25 mm, and the test point was the part between 0.25−1.75 mm from the upper surface of the test specimen.

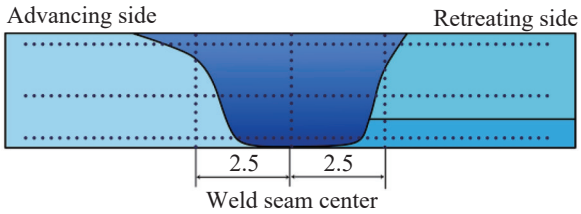

Fig. 3 Schematic diagram of hardness test point (mm)

2 Results and discussion

2.1 Tensile properties

The approximate welding parameter range was determined according to the pre-experiment. Tensile properties and mathematical statistics results based on the OE are shown in Table 2 and Table 3. Fig. 4 shows the relationship between the mean value of the welding coefficient and the welding parameters. The welding coefficient was based on the tensile strength of the thin sheet. Among all the parameters, the welding speed has the most significant extreme difference, indicating that its influence on the welding strength is greater than the rotational speed and the shoulder plunge depth.

The tensile property increases first and then decreases with the increased shoulder plunge depth. The influence trend of rotational speed and welding speed on the tensile property was similar. With the increase of parameters, the strength first increases, then decreases, and finally increases. The reasonable ratio could still obtain appropriate welding heat input when the rotational and welding speeds were high. If the shoulder plunge depth was also appropriate, relatively high tensile properties could also be obtained.

The optimal welding process parameter was 1100 r/min-300 mm/min−0.15 mm by calculating the average tensile properties of each factor at different levels. A verification

Table 2 Orthogonal experimental designed table

No.	Rotational speed /(r·min^{-1})	Welding speed /(mm·min^{-1})	Shoulder plunge depth/mm	Welding coefficient (%)
1	800	100	0.05	30.32
2	800	200	0.10	31.57
3	800	300	0.15	76.40
4	800	400	0.20	76.78
5	800	500	0.25	89.23
6	1 100	100	0.10	88.04
7	1 100	200	0.15	94.40
8	1 100	300	0.20	95.64
9	1 100	400	0.25	87.93
10	1 100	500	0.05	45.99
11	1 400	100	0.15	52.77
12	1 400	200	0.20	94.99
13	1 400	300	0.25	87.77
14	1 400	400	0.05	72.52
15	1 400	500	0.10	62.81
16	1 700	100	0.20	53.91
17	1 700	200	0.25	78.70
18	1 700	300	0.05	68.48
19	1 700	400	0.10	32.35
20	1 700	500	0.15	94.96
21	2000	100	0.25	49.20
22	2000	200	0.05	73.27
23	2000	300	0.10	88.67
24	2000	400	0.15	87.37
25	2000	500	0.20	80.23

experiment was performed to verify the result. The verification experiment was set 3 times, and the tensile strength reached 95.27%, 97.09 %, and 95.84 % (an average of 96.07%) of the thin BM, respectively.

Table 3 Mathematical statistics of orthogonal experimental results

Parameter	Rotational speed	Welding speed	Shoulder plunge depth
Mean value 1	61.8%	55.7%	59.0%
Mean value 2	82.4%*	74.8%	60.7%
Mean value 3	74.2%	83.4%*	81.2%*
Mean value 4	65.7%	71.4%	80.3%
Mean value 5	75.7%	74.6%	78.6%
Extreme difference	20.6%	27.7%	22.2%
Optimized parameters	1 100 r/min	300 mm/min	0.15 mm

2.2 Macro- and Microstructure results

The macroscopic surfaces of the specimens obtained with different parameters were observed, and the results are shown in Fig. 5. The weld seam surfaces were relatively flat, like similar welding, due to the addition of SBM. As shown in Fig. 5a, the surface was uneven when the heat input was low, and furrow defects appeared. The thermoplastic metal was less under the welding parameter with low rotational speed and small shoulder plunge depth, and the flow was insufficient[20]. The weld seam surface morphology improved when the welding heat input was increased with still small shoulder plunge depth, but wrinkles formed, as shown in Fig. 5b. The weld seam surface morphology further improved with the increased shoulder plunge depth, but the flash on the retreating side (RS) was also significantly increased, as shown in Fig. 5c. If the shoulder plunge depth was sufficient, appropriately increasing the rotational speed could make the surface of the weld seam smoother. Fig. 5e shows that reasonable shoulder plunge depth adjustment could still obtain a better-welded joint when the rotational and welding speeds were high. Fig. 5f shows the surface under the highest heat input parameters. There were flashes on the RS and the severe weld seam collapse.

Fig.6 shows a cross-section and detailed microstruc-

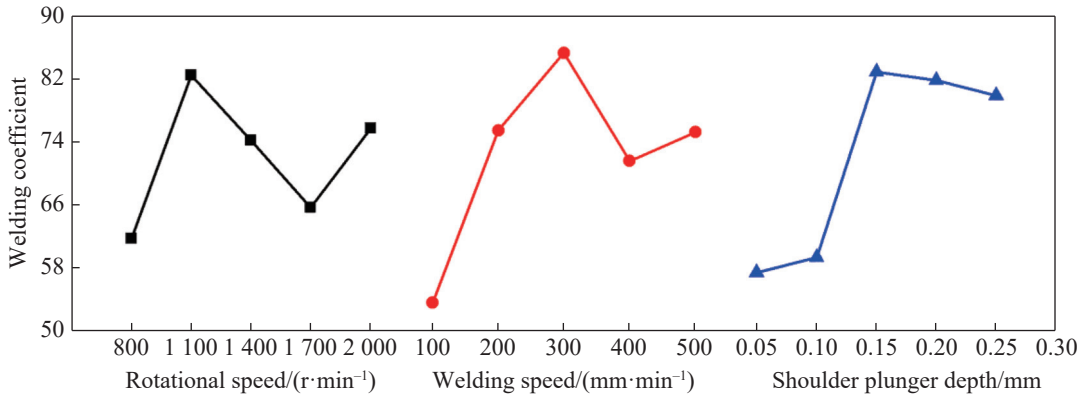

Fig. 4 The relationship between the mean value of welding coefficient and welding parameters

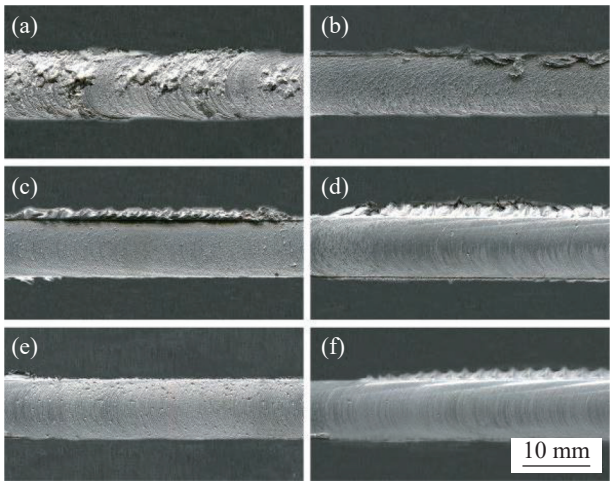

Fig. 5 Macroscopic morphology of weld surface of part of specimens (a) 800 r/min−200 mm/min−0.10 mm (b) 1100 r/min−100 mm/min−0.10 mm (c) 1100 r/min−300 mm/min−0.20 mm (d) 1400 r/min−200 mm/min−0.20 mm (e) 1700 r/min−500 mm/min−0.15 mm (f) 2000 r/min−100 mm/min−0.25 mm

tures of the weld seam under the parameter of 1 100 r/min−300 mm/min−0.15 mm. The left side is the advancing side (AS), and the right side is the RS. The 1 + 2 structure weld consists of the BMs and SBM, and there are four typical zones: weld nugget zone (WNZ), thermo-mechanically affected zone (TMAZ), HAZ, and BM.

In this 1 + 2 structure joint, the center of the WNZ was directly subjected to the mechanical stirring action of the pin, and the three sheets in this area were fused. Nevertheless, the thin sheet and supporting sheets were not fused near the TMAZ at a certain distance from the center of the WNZ. Compared with the traditional 1+1 joint structure, the hook defect in the joint of the 1 + 2 structure makes the 1.5 mm sheet slightly thinner in the dashed frame area in Fig. 6. The reason is that during the welding process, the thread on the pin drove the thin sheet material to flow downward and accumulate on the supporting sheet. Although this thinning reduces the mechanical properties of the region, at the same time, the grains in the region are refined, the material is strengthened, and a higher tensile strength of the joint can still be obtained[21]. It is worth noting that related studies have shown that this thinning phenomenon can be suppressed by reducing the rotation speed and increasing the welding speed[22, 23]. In addition, higher rotational speed or lower welding speed will increase the heat input and aggravate the softening of HAZ, reducing the joint tensile strength. Therefore, a smaller heat input should be used to improve the tensile strength of the welded joint. However, the friction heat generation and the stirring effect were weakened if with low heat input, resulting in insufficient material fusion. In this condition, the tunnel defects were prone to occur, as shown in Fig. 7.

The thinning phenomenon also often occurs in the lap FSWs[18 − 19]. The center of the WNZ was directly subjected to the mechanical stirring action of the pin, and the three sheets in this area were fused. Nevertheless, the thin sheet and supporting sheets were not fused near the TMAZ at a certain distance from the center of the WNZ. At the same time, the thread of the pin drove the thin sheet material to flow to the supporting sheet and accumulate on the supporting sheet.

The crystal grains of the BM were in the form of long

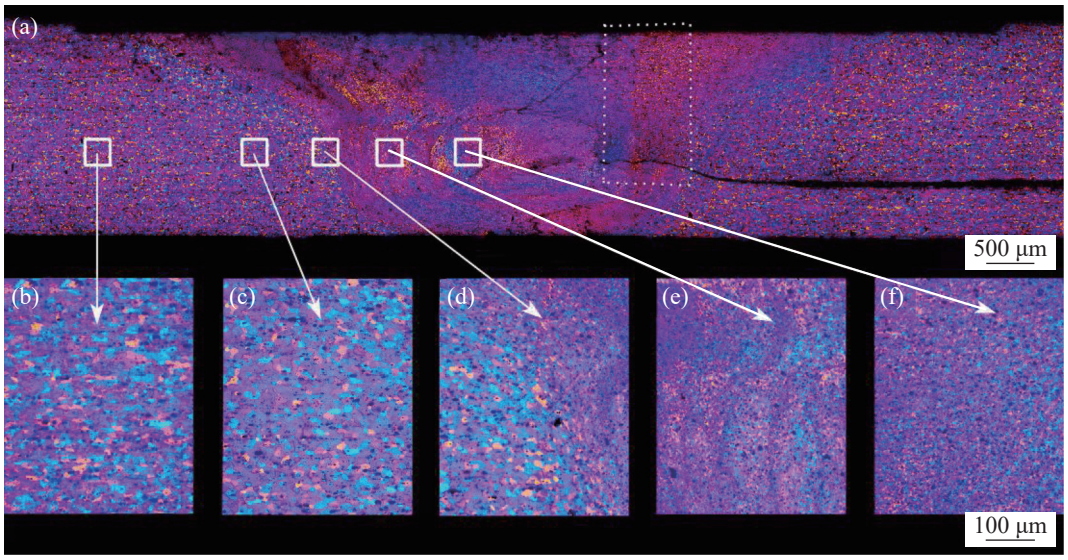

Fig. 6 Cross-section detailed microstructures of weld seam under 1100 r/min−300 mm/min−0.20 mm (a) Cross-section (b) BM (c) HAZ (d) TMAZ (e) Onion ring and (f) WNZ

Fig. 7 Schematic diagram of tunnel defects with improper parameters

and narrow fibers due to the rolling process, as shown in Fig. 6b. Comparatively, the grain sizes in the HAZ are more significant than those in the BM, as shown in Fig. 6c. The HAZ grain size is larger than that of BM because the HAZ is only affected by heat input and not mechanical stirring. Fig. 6d shows a clear boundary position between the TMAZ and the WNZ on the AS, while the boundary on the RS is more blurred. This is because, on the AS, the plastic flow direction of weld metal is opposite to that of base metal, resulting in prodigious relative deformation. On the contrary, there is the same plastic flow direction between the weld metal and the BM on the RS. The deformation between weld metal and the base metal is practically smooth.

An onion ring structure was formed on the AS of the WNZ, as shown in Fig. 6e. The essence of the onion ring is the trajectory produced by the stirring pin driving the softening layer to flow during the rotation, and relative movement, friction, and overlap with the upper softening layer. Onion rings have alternate bright and dark rings. The gap between two consecutive rings was more at center than at the outer edge. The grains in WNZ are finer than in BMs, as shown in Fig. 6f. The WNZ underwent recrystallization through heat input and mechanical stirring, resulting in refined equiaxed recrystallized grains.

A metallographic cross-section of the fractured specimen was made under 1 100 r/min−300 mm/min−0.15 mm to determine the weakest part, as shown in Fig. 8. The dashed line (a) corresponds to the edge position of the weld tool shoulder, and the dashed line (b) is the boundary between the HAZ and the TMAZ. The specimen fractured in the HAZ of a 1.5 mm thick sheet. Although there is a sheet thinning phenomenon at the dashed line frame (c), where slightly necked during a tensile test, the weakest part of the joint is HAZ, the necking is more prominent in the HAZ, where the fracture occurred.

Fig.9 shows the hardness distribution in the longitudinal and transverse direction of the joint. The hardness in the WNZ is higher than that in other zones. On the outside of WNZ, the hardness decreased from top to bottom, and the hardness on the AS side was higher than that of the RS side. The optimized high-performance joint fractured in the 1.5 mm thick sheet HAZ but not in the thinning area (Fig. 8). The reason is that the grains of the specimen in the WNZ and the TMAZ were significantly refined, and the hardness was improved. This coincides with the “W”-shape hardness distribution of the specimen cross-section. The hardness distribution cloud diagram shown in Fig. 10 also shows a similar result. In the cross-section of the joint, the hardness of HAZ is significantly lower than that of other zones, so the strength of HAZ is the lowest. This shows that the weakest part of new joint structure is HAZ, which is similar to traditional FSW.

Fig. 11 shows the hardness comparison of three typical specimens with suitable mechanical properties and welding formation under different welding parameters. The hardness distribution of the three specimens is similar. The HAZ

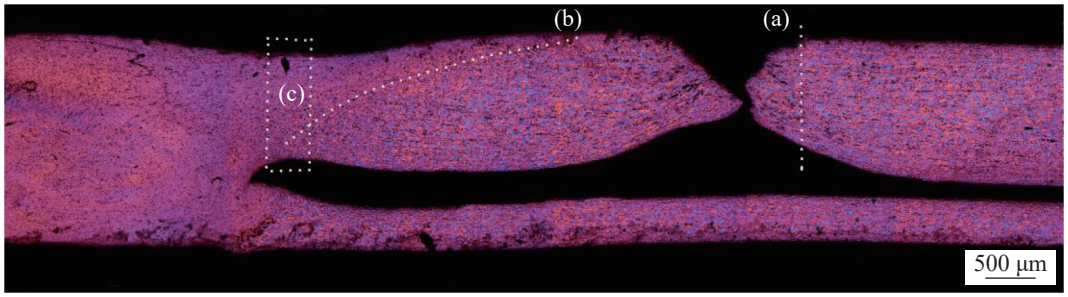

Fig. 8 Metallographic diagram of the cross-section of weld under the parameters of 1 100 r/min−300 mm/min−0.15 mm

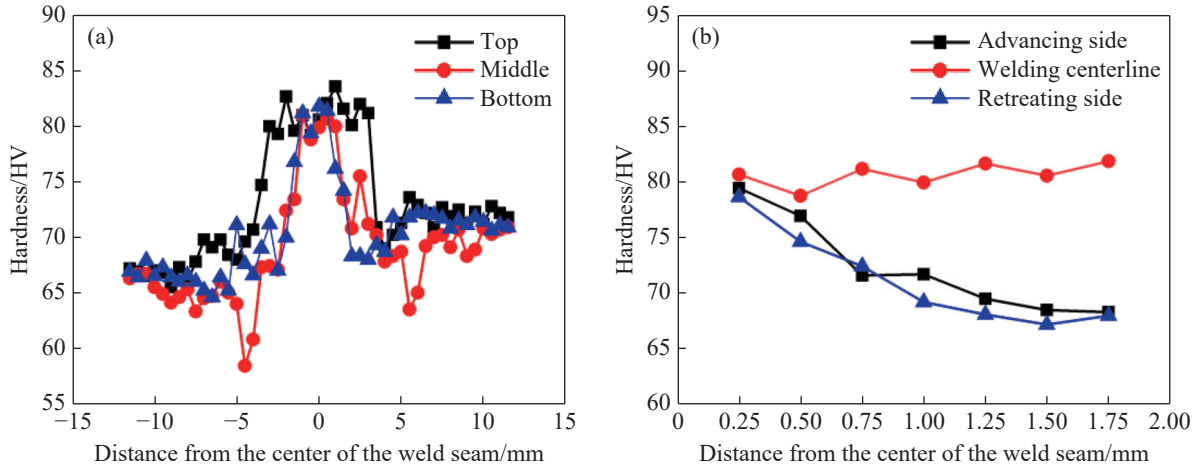

Fig. 9 The schematic diagram of hardness distribution at different positions in the transverse direction when the parameter is 1 100 r/min−300 mm/min−0.15 mm (a) Horizontal distribution (b) Longitudinal direction

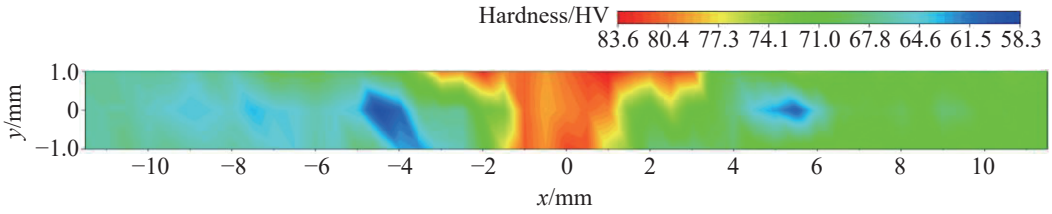

Fig. 10 Cloud diagram of hardness distribution in transverse section of 1 100 r/min−300 mm/min−0.20 mm specimen

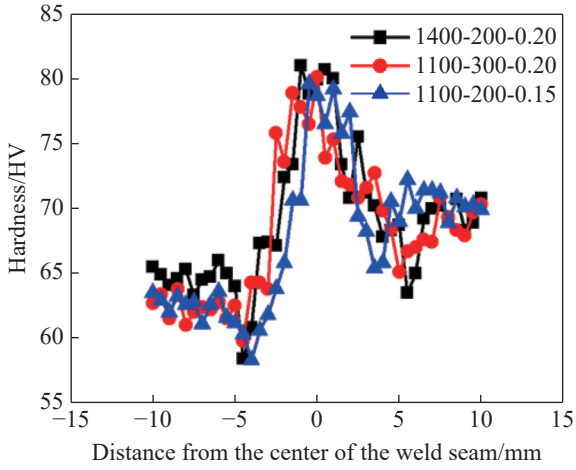

Fig. 11 Schematic diagram of hardness distribution in the middle section of specimens

softening degree of 1 100 r/min−300 mm/min−0.15 mm is lower than the other two specimens. Under this parameter, the line heat input was sufficient to achieve the material's recrystallization, and lower heat input decreased the softening degree in HAZ.

Fig. 12 shows the fracture surface of the tensile speci-

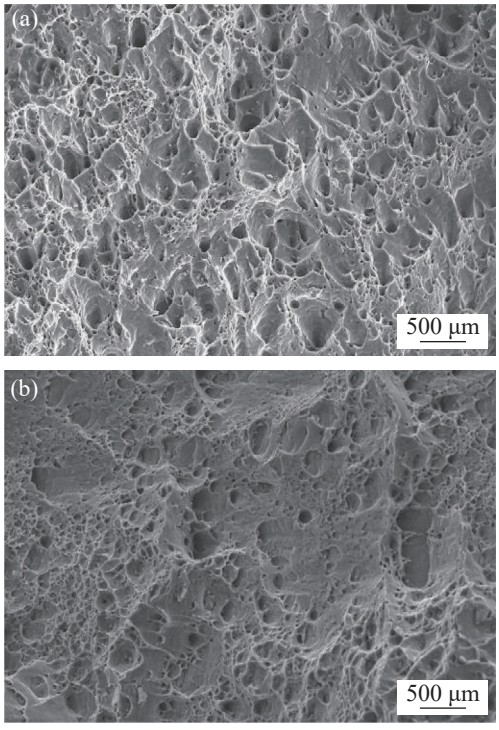

Fig. 12 Fracture morphology of tensile specimen (a) BM and (b) Welded joint

mens of the BM and welded specimens. Many dimples can be seen on the fracture surface of the BM, which indicates that it is a ductile fracture. There are dimples and tearing edges on the fracture surface of welded joints, and the fracture form is a mixed fracture where ductile fracture accounts for more.

3 Conclusions

(1) The new joint designed in this research has achieved good results for the FSW of aluminum alloys of unequal thickness. The optimized welding process parameters were 1 100 r/min−300 mm/min−0.15 mm, the specimen fractured in the HAZ in the tensile test.

(2) Because the WNZ and the TMAZ were subjected to heat input and mechanical stirring, the microstructure was recrystallized, and the grains were refined. The heat input affected the HAZ, and the grains were slightly coarser than the BM.

(3) Due to the recrystallization of WNZ, the grains were finer and the material was strengthened. Therefore, the thinning phenomenon occurring here does not reduce the tensile strength of the welded joint. And it still fractured in the HAZ in the tensile test.

(4) The overall hardness distribution of the welded joint cross-section showed a 'W'-shape, in which the hardness of the WNZ was the highest and the HAZ was the lowest. The HAZ was the weakest part of the entire welded joint. When the welding parameters are appropriate, the specimen fractured in the HAZ in the tensile test.

References

[1] Chang Y F, Lei Z, Wang X Y. Characteristic of laser-MIG hybrid welding with filling additional cold wire for aluminum alloy. China Welding, 2018, 27(3):35 − 41.

[2] Li M S, Zhang C Q, Wang D Y, et al. Friction stir spot welding of aluminum and copper: a review. Materials, 2020, 13(1):156.

[3] Wang W Q, Wang S Y, Zhang X E, et al. Enhanced aluminum alloy-polymer friction stir welding joints by introducing micro-textures. Materials Letters, 2021, 295(1):129872.

[4] Cao X, Wallace W, Poon C, et al. Research and progress in laser welding of wrought aluminum alloys. I. Laser welding processes. Materials and Manufacturing Processes, 2003, 18(1):1 − 22.

[5] Garware M, Kridli G T, Mallick P K. Tensile and fatigue behavior of friction-stir welded tailor-welded blank of aluminum alloy 5754. Journal of Materials Engineering and Performance, 2010, 19(8):1161 − 1171.

[6] Morishita Y, Kado T, Abe S, et al. Role of counterpunch for square-cup drawing of tailored blank composed of thick/thin sheets. Journal of Materials Processing Technology, 2012, 212(10):2102 − 2108.

[7] Lin Z C, Zhao Y Q, Yan D J, et al. Study on microstructure and mechanical properties of new generation high-magnesium aluminum alloy cross-welded joints by friction stir welding-friction stir welding. Transactions of the China Welding Institution, 2022, 43(10):24 − 30. (in Chinese)

[8] Wang H X, Zhang J Y, Wang B, et al. Influence of surface enhanced treatment on microstructure and fatigue performance of 6005A aluminum alloy welded joint. Journal of Manufacturing Processes, 2020, 60:563 − 572.

[9] Wang Y Y, Yang X N, Shi S Y, et al. Laser welding 6061 aluminum alloy with laser cladding powder. Journal of Laser Applications, 2021, 33:022006.

[10] Yu S R, Fan D, Xiong J H, et al. CO_2 laser welding of tailored 5A02 aluminum alloy sheets with different thickness using filler powder. Transactions of the China Welding Institution, 2007, 28(3):25 − 28. (in Chinese)

[11] Gao S K, Zhou L, Zhang X M, et al. Microstructure and properties of friction stir welded joints for 6061-T6/7075-T6 dissimilar aluminum alloy. Transactions of the China Welding Institution, 2022, 43(6):35 − 42. (in Chinese)

[12] Patel V, Li W Y, Wang G Q, et al. Friction stir welding of dissimilar aluminum alloy combinations: state-of-the-art. Metals, 2019, 9(3):1 − 19.

[13] Kim N K, Kim B C, An Y G, et al. The effect of material arrangement on mechanical properties in friction stir welded dissimilar A5052/A5J32 aluminum alloys. Metals and Materials International, 2009, 15(4):671 − 675.

[14] Buffa G, Fratini L, Hua J, et al. Friction stir welding of tailored blanks: investigation on process feasibility. CIRP Annals-Manufacturing Technology, 2006, 55:279 − 282.

[15] Fratini L, Buffa G, Shivpuri R. Improving friction stir welding of blanks of different thicknesses. Materials Science and Engineering A, 2007, 459:209 − 215.

[16] Avinash P, Manikandan M, Arivazhagan N, et al. Friction stir welded butt joints of AA2024T3 and AA7075 T6 aluminum alloys. Procedia Engineering, 2014, 75:98 − 102.

[17] Padmanaban R, Ratna K V, Balusamyc V. Numerical simulation of temperature distribution and material flow during friction stir welding of dissimilar aluminum alloys. Procedia Engineering, 2014, 97:854 − 863.

[18] Yadava M K, Mishra R S, Chen Y L. Study of friction stir joining of thin aluminum sheets in lap joint configuration. Science and Technology of Welding and Joining, 2010, 15:70 − 75.

[19] Kimapong K, Watanabe T. Effect of welding process parameters on mechanical property of FSW lap joint between aluminum alloy and steel. Materials Transactions, 2005, 46(10):2211 − 2217.

[20] Zhao Y, Ye Y L, Yan K. Microstructure and mechanical properties of friction stir welding joint of pure copper. Advanced Materials Research, 2011, 418:1520 − 1523.

[21] Monajati H, Zoghlami M, Tongne A. Assessing microstructure-local mechanical properties in friction stir welded 6082-t6 aluminum alloy. Metals, 2020, 10(9):1244.

[22] Tan Y B, Wang X M, Ma M. A study on microstructure and mechanical properties of AA 3003 aluminum alloy joints by underwater friction stir welding. Materials Characterization, 2017, 127:41 − 52.

[23] Imam M, Sun Y, Fujii H. Microstructural characteristics and mechanical properties of friction stir welded thick 5083 aluminum alloy. Metallurgical and Materials Transactions A, 2016, 48:208 − 229.